

1 **Last ice sheet recession and landscape emergence above sea level in east-central Sweden, evaluated**
2 **using *in situ* cosmogenic ¹⁴C from quartz**

3

4 Bradley W. Goodfellow^{1*}

5 Arjen P. Stroeven^{2,3}

6 Nathaniel A. Lifton^{4,5}

7 Jakob Heyman⁶

8 Alexander Lewerentz¹

9 Kristina Hippe⁷

10 Jens-Ove Näslund⁸

11 Marc W. Caffee^{4,5}

12

13 ¹Geological Survey of Sweden

14 ²Department of Physical Geography, Stockholm University

15 ³Bolin Centre for Climate Research, Stockholm University

16 ⁴Department of Earth, Atmospheric, and Planetary Sciences, Purdue University

17 ⁵Department of Physics and Astronomy, Purdue University

18 ⁶Department of Earth Sciences, University of Gothenburg

19 ⁷Umweltplanung Dr. Klimsa

20 ⁸Swedish Nuclear Fuel and Waste Management Company (SKB)

21

22 *Corresponding author: bradley.goodfellow@sgu.se

23

24 **Abstract**

25 *In situ* cosmogenic ¹⁴C (*in situ* ¹⁴C) in quartz provides a recently developed tool to date exposure of
26 bedrock surfaces up to ~25,000 years. From outcrops located in east-central Sweden, we test the
27 accuracy of *in situ* ¹⁴C dating against (i) a relative sea level (RSL) curve constructed from radiocarbon
28 dating of organic material in isolation basins, and (ii) the timing of local deglaciation constructed from
29 a clay varve chronology complemented with traditional radiocarbon dating. Five samples of granitoid
30 bedrock were taken along an elevation transect extending southwestwards from the Baltic Sea coast
31 near Forsmark. Because these samples derive from bedrock outcrops positioned below the highest
32 postglacial shoreline, they target the timing of progressive landscape emergence above sea level. In
33 contrast, *in situ* ¹⁴C concentrations in an additional five samples taken from granitoid outcrops above
34 the highest postglacial shoreline, located 100 km west of Forsmark, should reflect local deglaciation

35 ages. The ten *in situ* ^{14}C measurements provide robust age constraints that, within uncertainties,
36 compare favorably with the RSL curve and with the local deglaciation chronology. These data
37 demonstrate the utility of *in situ* ^{14}C to accurately date ice sheet deglaciation, and durations of
38 postglacial exposure, in regions where cosmogenic ^{10}Be and ^{26}Al routinely return complex exposure
39 results.

40 **1. Introduction**

41 The pacing of retreat of ice sheets in North America and Eurasia since their maximum expansion
42 during the last glaciation remains an active research field (e.g., Hughes et al., 2016; Stroeven et al.,
43 2016; Patton et al., 2017; Dalton et al., 2020, 2023). Understanding the triggers and processes causing
44 the demise of these ephemeral ice sheets yields the best blueprint for understanding the future
45 behavior of the Greenland and Antarctic ice sheets in a warming climate. Coupling the behavior of
46 deglaciating ice sheets over the course of the Late Glacial and early Holocene to increasingly precise
47 climate reconstructions, including climatic events, requires increased precision in ice sheet
48 reconstructions (e.g., Bradwell et al., 2021). Precision can be enhanced through coupling
49 geomorphological mapping of ice sheet margins (such as moraines, grounding zone wedges, lateral
50 meltwater channels, and ice-dammed lake shorelines and spillways) with numerical field constraints
51 from a diverse array of dating techniques (e.g., Stroeven et al., 2016; Bradwell et al., 2021; Regn  l et
52 al., 2023).

53 Ice sheet reconstructions, especially in North America, have become highly detailed through
54 radiocarbon dating (Dyke et al., 2002; Dalton et al., 2020). With the advance of offshore imaging of
55 glacial geomorphology (Greenwood et al., 2017, 2021; Bradwell et al., 2021), radiocarbon dating has
56 received a renewed upswing in recent years (e.g., Dalton et al., 2020; Bradwell et al., 2021). However,
57 large landscape areas lack radiocarbon age constraints on ice sheet retreat because of an absence of
58 datable organic material. Fortunately, optically stimulated luminescence ages on buried sand layers
59 (e.g., Alexanderson et al., 2022) and cosmogenic nuclide apparent exposure ages on exposed bedrock
60 and erratics have narrowed some of the gaps (e.g., Hughes et al., 2016; Stroeven et al., 2016; Dalton et
61 al., 2023). In studies using cosmogenic nuclides, an ‘apparent’ exposure age is derived from a simple
62 calculation from the nuclide concentration under consideration (Lal, 1991; Gosse and Phillips, 2001).
63 Correctly interpreting the exposure age relies on modelling that considers geological factors that can
64 reduce the nuclide concentration relative to the time since initial subaerial exposure (such as erosion
65 and burial by glacial ice, water, snow, and/or soil; Gosse and Phillips, 2001; Schildgen et al., 2005; Ivy-
66 Ochs and Kober, 2008). Exposure dating is the only technique available in regions where ice sheet
67 erosion has left the surface bare or covered by a thin drape of till. Kleman et al. (2008) show that for
68 Fennoscandia, these conditions are widespread in coastal regions where ice accelerated towards its

69 streaming sectors and where wave wash during glacial rebound further thinned or removed pre-
70 existing sediment covers.

71 Coastal sectors in formerly glaciated regions provide sites important to the study of paleoglaciology.
72 They offer an abundance of bedrock exposures from which patterns and processes of subglacial
73 erosion can be studied through cosmogenic nuclide exposure dating (e.g., Hall et al., 2020). Also,
74 because of the interplay with postglacial sea level, coastal areas yield data on glacioisostatic rebound
75 that are critical to geodynamic modelling of Earth rheology and thicknesses of former ice sheets (e.g.,
76 Lambeck et al. (1998, 2010) and Patton et al. (2017), for Fennoscandian examples). Geodynamic
77 models require validation against measurements of vertical crustal motion (Steffen and Wu, 2011),
78 such as those provided by recent global positioning system (GPS) measurements (e.g., Lidberg et al.,
79 2010) and postglacial records of crustal rebound afforded by relative sea level (RSL) curves (e.g., Pålsson
80 and Andersson, 2005). The construction of RSL curves, detailing the history of land surface emergence
81 from sea level, is traditionally done using either sediments accumulated in isolation basins at different
82 elevations above sea level or by dating uplifted gravel beach ridges. Typically, isolation basins, and their
83 sediments, show a progression from marine, to brackish, and finally to freshwater environments as
84 they are uplifted through tidal levels (Long et al., 2011). Histories of land uplift above sea level are
85 documented using micro- and macrofossil analyses of isolation basin sediments and radiocarbon
86 dating on macrofossils (Romundset et al., 2011). Uplifted beach ridges can be radiocarbon dated from
87 a variety of materials (Blake, 1993) but most confidently from driftwood, whalebone, and shells (e.g.,
88 Dyke et al., 1992). Gravel beach ridges have also been investigated using OSL and ^{10}Be exposure dating
89 even though, other than the highest beach ridge, they may be prone to clast reworking (Briner et al.,
90 2006; Simkins et al., 2013; Bierman et al., 2018). A distinct advantage of constructing RSL curves using
91 cosmogenic nuclides is that land surface emergence above sea level may be additionally dated from
92 boulders (Briner et al., 2006) or bedrock (Bierman et al., 2018).

93 The potential for cosmogenic surface exposure dating of last ice sheet retreat in recently glaciated low-
94 relief cratonic landscapes would seemingly be high because of the frequent outcropping of glacially
95 sculpted quartz-bearing crystalline bedrock. However, the ice sheet may have been either non-erosive
96 or erosion was insufficiently deep to remove all the cosmogenic nuclide inventory from previous
97 exposure periods. Apparent ages are therefore often older than indicated by radiocarbon dating
98 (Heyman et al., 2011; Stroeven et al., 2016) because they include a component of nuclide inheritance.
99 Apparent ages younger than indicated by radiocarbon dating can also occur if sampled rock surfaces
100 have been shielded, for example by sediments, following deglaciation. Concentrations of ^{10}Be and ^{26}Al ,
101 in either bedrock or erratic boulders, often reflect complex exposure histories rather than simple
102 deglacial exposure durations (Heyman et al., 2011; Stroeven et al., 2016).

103 In this study we use ^{14}C produced *in situ* in quartz-bearing bedrock (*in situ* ^{14}C) because it potentially
104 circumvents an overt reliance on the need for deep erosion (>3 m) to remove the inherited signal from
105 previous exposure periods (Gosse and Phillips, 2001). Because of its short half-life of 5700 ± 30 years,
106 inherited *in situ* ^{14}C will decay if ice sheet burial at investigated sites during the last glacial phase
107 (marine isotope stage 2; MIS2) exceeded 25-30 ka, that is, ca. 5 half-lives (Briner et al., 2014).

108 Some studies assessing changes in glacier and ice sheet extents over Late Glacial to Holocene
109 timescales have used *in situ* ^{14}C (Miller et al., 2006; Fogwill et al., 2014; Hippe et al., 2014;
110 Schweinsberg et al., 2018; Pendleton et al., 2019; Young et al., 2021; Schimmelpfennig et al., 2022). In
111 these studies, *in situ* ^{14}C has been applied with other nuclides with longer half-lives, in particular ^{10}Be ,
112 to unravel complex histories of glacier advance and retreat (e.g., Goehring et al., 2011) and spatial
113 patterns in glacial erosion in mountainous terrain (e.g., Steinemann et al., 2021). Extensive regions
114 formerly covered by ice sheets are characterized by low relief and low elevation terrain. The
115 effectiveness of *in situ* ^{14}C in dating ice sheet retreat in these non-alpine settings and in quantifying
116 shoreline displacement from bedrock samples has not been previously assessed. The aim of this study
117 is therefore to validate the use of ^{14}C formed *in situ* in bedrock as a reliable chronometer by evaluating
118 its performance in duplicating (i) a previously-established Holocene RSL curve based on radiocarbon
119 dating (Hedenström and Risberg, 2003; SKB, 2020) and (ii) the timing of deglaciation above the highest
120 (post-glacial) shoreline in nearby east-central Sweden according to reconstructions of deglaciation of
121 the last ice sheet (Hughes et al., 2016; Stroeven et al., 2016).

122

123 **2. Study Area**

124 Our study is focused on a region that includes low elevation, low relief, Forsmark-Uppland and
125 adjoining higher elevation and relief Dalarna-Gävleborg in east-central Sweden (Fig. 1). This region was
126 selected because Forsmark is the location of a planned geological repository for spent nuclear fuel
127 (e.g., SKB 2022). As such, this region has been intensively studied and has a wealth of geologic data
128 relevant to our study. This includes in-depth analyses of bedrock and environmental properties,
129 including influences of glacial and postglacial processes (e.g., Lönnqvist and Hökmark, 2013; Hall et al.,
130 2019; Moon et al., 2020; SKB, 2020).

131 From spatio-temporal ice sheet reconstructions by Kleman et al. (2008), the study area was glaciated
132 16-20 times for a total duration of c. 330 kyr over the past 1 Ma. The last deglaciation of the study area
133 is well-constrained by two recent reconstructions that differ in their approach (Hughes et al., 2016;
134 Stroeven et al., 2016). The Hughes et al. (2016) reconstruction relies primarily upon chronological
135 constraints supplied from radiocarbon, thermal luminescence, optically stimulated luminescence
136 (OSL), infrared stimulated luminescence, electron spin resonance, terrestrial cosmogenic nuclide

137 (TCN), and U-series dating. Published landform data, mostly with respect to end moraines and
138 generally accepted correlations of ice-margin positions between individual moraines, provide
139 complementary evidence. In contrast, the Stroeven et al. (2016) reconstruction combines
140 geomorphological constraints for ice sheet margin outlines, including ice-marginal depositional
141 landforms and meltwater channels, ice-dammed lakes, eskers, lineations, and striae, with
142 chronological constraints supplied by radiocarbon, varve, OSL, and TCN dating. Whereas Hughes et al.
143 (2016) reconstruct ice sheet retreat every 1 ka, and for every ice margin plot its position as “most
144 credible”, “min”, and “max”, Stroeven et al. (2016) present ice margin positions for every 100 years
145 inside the Younger Dryas standstill position (Stroeven et al., 2015). These marginal positions are
146 temporally and spatially defined by the “Swedish Time Scale” clay varve record along the Swedish east
147 coast (De Geer, 1935, 1940; Strömberg, 1989, 1994; Brunnberg, 1995; Wohlfarth et al., 1995). From
148 Stroeven et al. (2016), the last deglaciation of the study area occurred 10.8 ± 0.3 ka BP, which overlaps
149 the timing of deglaciation of the study area from Hughes et al. (2016), within uncertainty (Fig. 1). The
150 highest postglacial shoreline in east-central Sweden is located at a present elevation of ~ 200 m a.s.l. in
151 Dalarna-Gävleborg, ~ 100 km west of Forsmark (SGU, 2015). The exposure duration of bedrock above
152 the highest postglacial shoreline represents the time since local deglaciation. Hence, *in situ* ^{14}C ages
153 from bedrock above the highest postglacial shoreline should conform to the reconstructed
154 deglaciation age of 10.8 ± 0.3 ka from Stroeven et al. (2016).

155 Below the highest postglacial shoreline, in the Forsmark-Uppland region, the last deglaciation
156 occurred in a marine environment and the landscape has progressively emerged above sea level
157 through postglacial isostatic uplift. A RSL curve constructed from radiocarbon dating of basal organic
158 sediments trapped in isolation basins along elevation transects describes the progressive emergence
159 of the Forsmark-Uppland landscape above sea level (Robertsson and Persson, 1989; Risberg, 1999;
160 Bergström, 2001; Hedenström and Risberg, 2003; Berglund, 2005; SKB, 2020). Ages calculated from *in*
161 *situ* ^{14}C from bedrock outcrops along an elevation transect would then mirror the Forsmark RSL curve
162 for their corresponding elevations (but be slightly older because of nuclide production through
163 shallow water before emergence).

164 A potential complication to the accurate exposure age dating of bedrock surfaces using *in situ* ^{14}C in
165 east-central Sweden is that the most recent period of ice sheet burial may not have been sufficiently
166 long to decay any *in situ* ^{14}C inventory inherited from prior exposure. Here, the extent of the
167 Fennoscandian Ice Sheet during interstadial MIS3 and the timing of ice advance across the Forsmark
168 region during late MIS3 are crucially important. Kleman et al. (2020) have identified ice-free conditions
169 around Idre (330 km NW, up-ice, of our study area; Fig. 1) between 55 ka and 35 ka, which implies
170 inundation of our study area by ice after 35 ka. Combined with a well-constrained final deglaciation
171 age of 10.8 ± 0.3 ka (Stroeven et al. 2016), it appears that our study area has most recently (during

172 MIS2) been inundated by glacial ice for at most 24 ka. This inference is in line with results from ice
173 sheet modelling indicating a 22 kyr duration of ice-cover at Forsmark during MIS2 (SKB, 2020).
174 Consequently, it is possible that *in situ* ¹⁴C concentrations may reflect subaerial exposure of bedrock in
175 our study area during MIS3 in addition to Holocene exposure, resulting in an offset towards older ages
176 relative to the RSL curve for Forsmark (Hedenström and Risberg, 2003; SKB, 2020) and the deglaciation
177 chronologies of Hughes et al. (2016) and Stroeve et al. (2016).

178

179 3. Methods

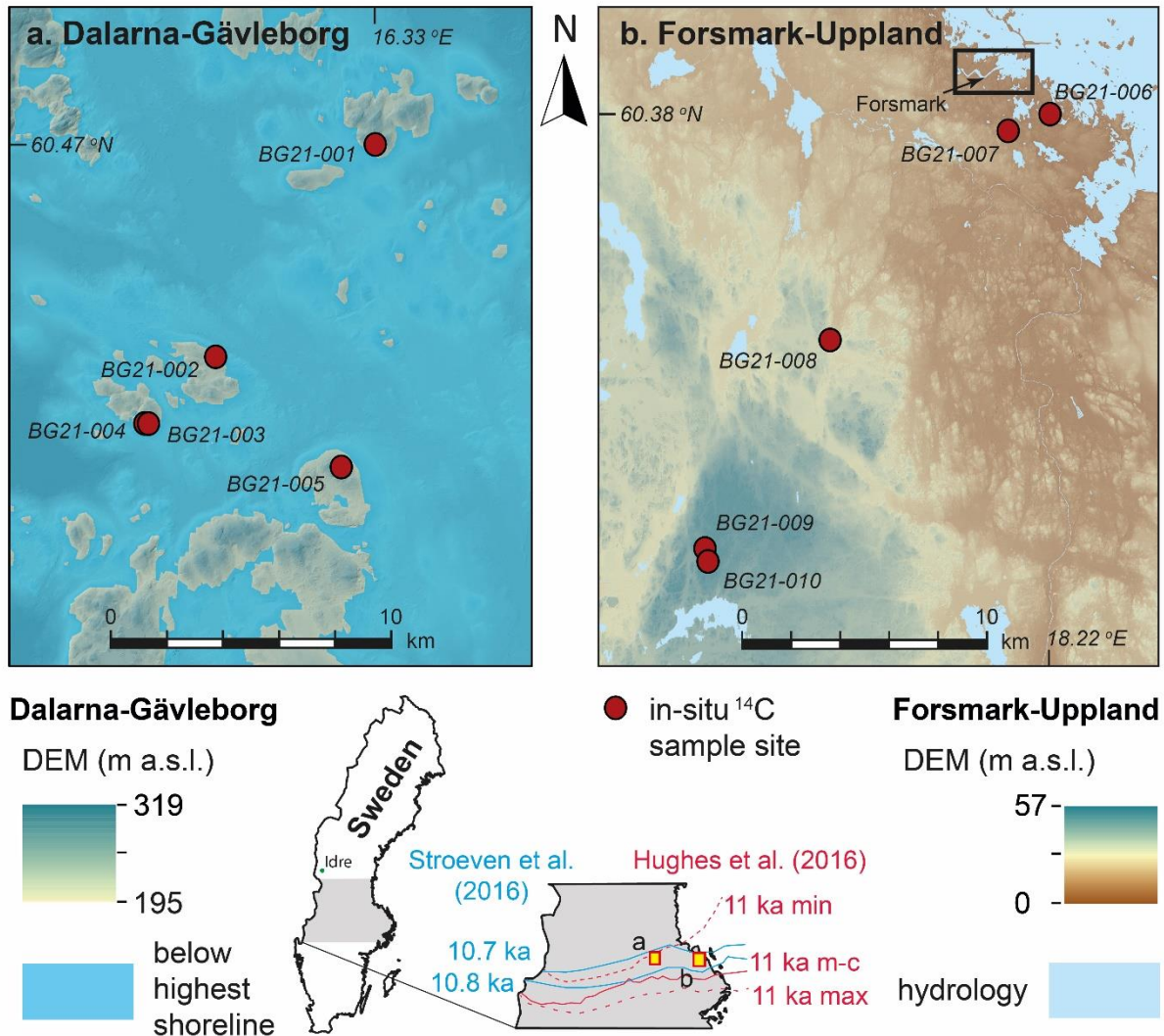
180 3.1. Sampling of bedrock outcrops for *in situ* ¹⁴C measurement

181 We used the following sampling strategy to evaluate the accuracy of bedrock exposure ages derived
182 from *in situ* ¹⁴C against the Forsmark RSL curve and the deglaciation of the last ice sheet in east-central
183 Sweden. A rigorous scheme was applied to ensure that we avoided sampling quartz altered through
184 hydrothermal processes that is likely to occur in major pegmatite intrusions, outcrops located in major
185 deformation zones, and outcrop-scale veins, fractures, and adjacent rock volumes. Consequently,
186 sampling was done on outcrops of metagranitoid from the early-Svecokarelian GDG-GSDG suite that
187 dominates the Bergslagen lithotectonic unit (Stephens and Jansson, 2020). A petrological examination
188 using transmitted light polarization microscopy was applied to thin sections to ascertain that the quartz
189 was unlikely to contain multi-fluid phase, vapour phase, or solid-phase inclusions. All samples were
190 collected using an angle grinder, which permits sampling of hard crystalline bedrock isolated from
191 outcrop edges, fractures, and quartz veins, and consistently limits sample thicknesses to 3 cm.

192 We collected a total of ten samples for *in situ* ¹⁴C analyses. Five of these were collected along a SW-NE
193 transect near Forsmark (Fig. 1b). These outcrops were chosen because they span an elevation gradient
194 of 9.4–56.0 m a.s.l. and exposure ages derived from *in situ* ¹⁴C can therefore be evaluated against the
195 Forsmark RSL curve. We collected a further five samples from locations above the highest shoreline (Fig.
196 1a) to determine the age of local deglaciation for comparison with published deglaciation chronologies
197 (Hughes et al., 2016; Stroeve et al., 2016). Sample locations were logged on a 2 m-resolution LiDAR
198 digital elevation model (DEM) displayed in ArcGIS 10 on a tablet computer. A GPS add-in tool in ArcGIS
199 10 was used to record positional data, within a horizontal precision of 2 m. The elevation of each sample
200 location was extracted from the DEM and has a precision of tens of centimetres. The influence of these
201 minor positional uncertainties on our ¹⁴C calculations is trivial and none of the sample sites is influenced
202 by topographic shielding that could reduce the accumulation of ¹⁴C in bedrock.

203 Each sampled bedrock outcrop formed a local topographic high, which minimizes the risk of burial by
204 soil and snow (Supplement 1). Moss mats were present on all sampled outcrops. Although we avoided

205 sampling bedrock that was moss-covered, we cannot be certain that moss mats did not formerly cover
 206 the sample sites. Given a compressed thickness of 0.5 cm and an estimated density of 0.7 g cm⁻³, this
 207 may have contributed to a shielding of the sampled rock surfaces of 0.35 g cm⁻², which is negligible and
 208 is therefore excluded from our age inferences.



209
 210 **Figure 1.** Sample locations for *in situ* ¹⁴C dating in **(a)** Dalarna-Gävleborg and **(b)** Forsmark-Uppland. The
 211 five Dalarna-Gävleborg sample sites are located on what were islands above the highest postglacial
 212 shoreline (shown), whereas the five sample sites from Forsmark-Uppland are located below the highest
 213 shoreline (not shown because the entire area was submerged). See inset maps for locations of panels a
 214 and b and for the 10.7 ka BP and 10.8 ka BP retreat isochrones (blue) from Stroeven et al. (2016) and 11
 215 ka BP (most-credible, minimum, and maximum) retreat isochrones (red) from Hughes et al. (2016). The
 216 rectangle in panel b approximately indicates the site selected for the planned geological repository for
 217 spent nuclear fuel at Forsmark. DEM with 2 m resolution, from LiDAR data, Lantmäteriet.

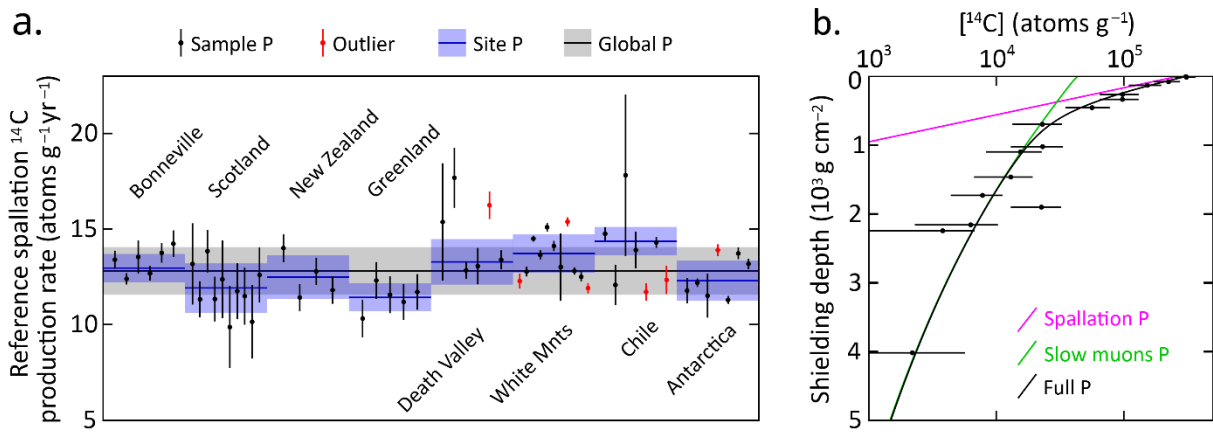
218 **3.2. Laboratory preparation for accelerator mass spectrometry (AMS)**

219 Samples were physically and chemically processed at the Purdue Rare Isotope Measurement Laboratory
220 (PRIME Lab) at Purdue University, U.S.A. Concentrations of *in situ* ^{14}C were determined from purified
221 quartz separates through automated procedures (Lifton et al., 2023). Approximately 5 g of quartz from
222 each sample was added to a degassed LiBO_2 flux in a re-usable 90% Pt/10% Rh sample boat and heated
223 to 500 °C for one hour in ca. 6.7 kPa of Research Purity O_2 to remove atmospheric contaminants, which
224 were discarded. The sample was then heated to 1100 °C for three hours to dissolve the quartz and
225 release the *in situ* ^{14}C , again in an atmosphere of ca. 6.7 kPa of Research Purity O_2 to oxidize any evolved
226 carbon species to CO_2 . The CO_2 from the 1100 °C step was then purified, measured quantitatively, and
227 converted to graphite for ^{14}C AMS measurement at PRIME Lab (Lifton et al., 2023). To test for data
228 reproducibility, sample BG21-002 was randomly selected to undergo laboratory preparation and AMS a
229 second time. Measured concentrations of *in situ* ^{14}C are calculated from the measured isotope ratios via
230 AMS following Hippe and Lifton (2014) (Table 1).

231 **3.3. Exposure age calculations**

232 The expage calculator version 202403 (<http://expage.github.io/calculator>) is used to calculate apparent
233 exposure ages. It is based on the original CRONUS calculator v. 2 (Balco et al., 2008), the LSDn production
234 rate scaling (Lifton et al., 2014), and the CRONUScalc calculator (Marrero et al., 2016), using the
235 geomagnetic framework of Lifton (2016) with the SHA.DIF.14k model for the last 14 kyr. Exposure ages
236 are calculated using resulting time-varying ^{14}C production rates accounting for decay and interpolated
237 to match the measured ^{14}C concentration. The production rate from muons is calibrated against the
238 Leymon High core ^{14}C data of Lupker et al. (2015) and the production rate from spallation is calibrated
239 against updated global ^{14}C production rate calibration data (Schimmelpfennig et al., 2012; Young et al.,
240 2014; Lifton et al., 2015; Borchers et al., 2016; Phillips et al., 2016; Koester and Lifton, 2023, corrigendum
241 in prep). This calibration is done iteratively for spallation and muons to reach convergence, using the
242 expage production rate calibration methods (Fig. 2).

243 Exposure age calculations along the Forsmark-Uppland transect account for ^{14}C production during
244 emergence through shallow water. Burial of sampled surfaces by snow is excluded from the age
245 calculations for all sample sites because we neither know how snow burial depths and durations vary
246 between sites nor vary through time. The effect of snow burial would be to slightly decrease cosmogenic
247 nuclide production in the underlying rock surface (Schildgen et al., 2005) and we have minimized this
248 effect through our sampling strategy.



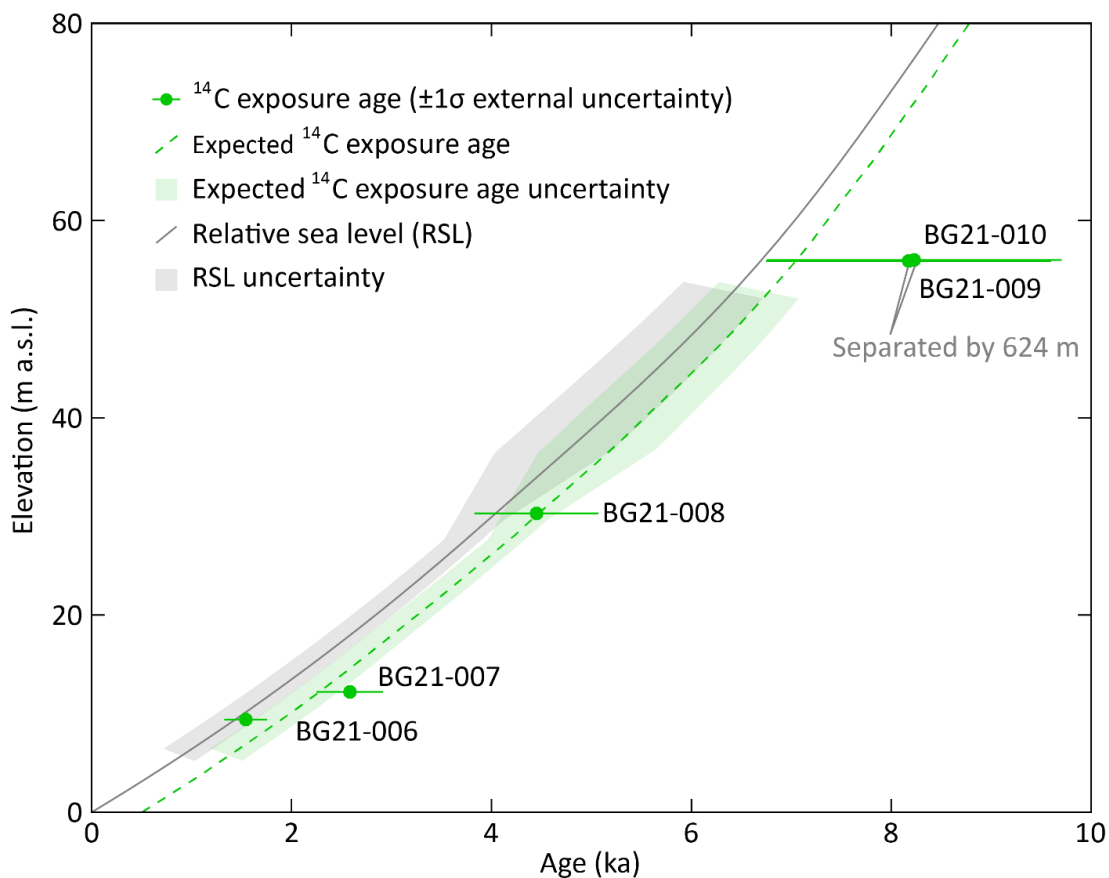
249 **Figure 2.** Production rate calibration of ^{14}C in quartz. **(a)** Reference spallation ^{14}C production rate
 250 calibration based on data from Schimmelpfennig et al. (2012), Young et al. (2014), Lifton et al. (2015),
 251 Borchers et al. (2016), and Phillips et al. (2016), corrected per Hippe and Lifton (2014) and compiled in
 252 Koester and Lifton (2023). An uncertainty-weighted production rate is calculated for each of the eight
 253 sites. Outliers, which are not included in the uncertainty-weighted production rates, are determined
 254 based on the requirement that there should be at least three samples yielding a reduced chi-square
 255 statistic (X_R^2) with a p-value of at least 0.05 for the assumption that the individual production rates from
 256 a site are derived from one normal distribution. For X_R^2 , but not the uncertainty-weighting, we use the
 257 largest of the sample-specific production rate uncertainty based on the ^{14}C concentration uncertainties
 258 and 5% of the sample production rate. This procedure does not punish samples with low measurement
 259 uncertainties, which otherwise risk exclusion as outliers. We adopt a global reference spallation ^{14}C
 260 production rate of 12.81 ± 1.25 atoms $\text{g}^{-1} \text{yr}^{-1}$, calculated as the arithmetic mean of the eight site
 261 production rates with the uncertainty being based on an uncertainty-weighted deviation of all included
 262 single sample production rates, excluding outliers. **(b)** Calibration of ^{14}C production rate from muons
 263 based on the data of Lupker et al. (2015). The calibration is based on the method used in the CRONUScalc
 264 calculator (Marrero et al., 2016; Phillips et al., 2016). The figure shows the best fit ^{14}C concentration
 265 profiles produced from spallation, slow muons, and full production. The best fit yields near zero
 266 production from fast muons (cf. Lupker et al., 2015). The production rate calibration has been carried
 267 out using the expage-202403 calculator in an iterative way to make the global reference spallation ^{14}C
 268 production rate converge with the production rate from muons.

269

270 4. Results

271 Analytical results for *in situ* ^{14}C samples and procedural blanks are presented in Table 1. The mean and
 272 standard deviation are used to correct measured ^{14}C sample inventories (Table 1) because procedural
 273 blanks are well-constrained during the analytical time frame. Inferred ages for the five *in situ* ^{14}C samples
 274 from the Forsmark-Uppland transect (i.e., below the highest postglacial shoreline) are shown relative to

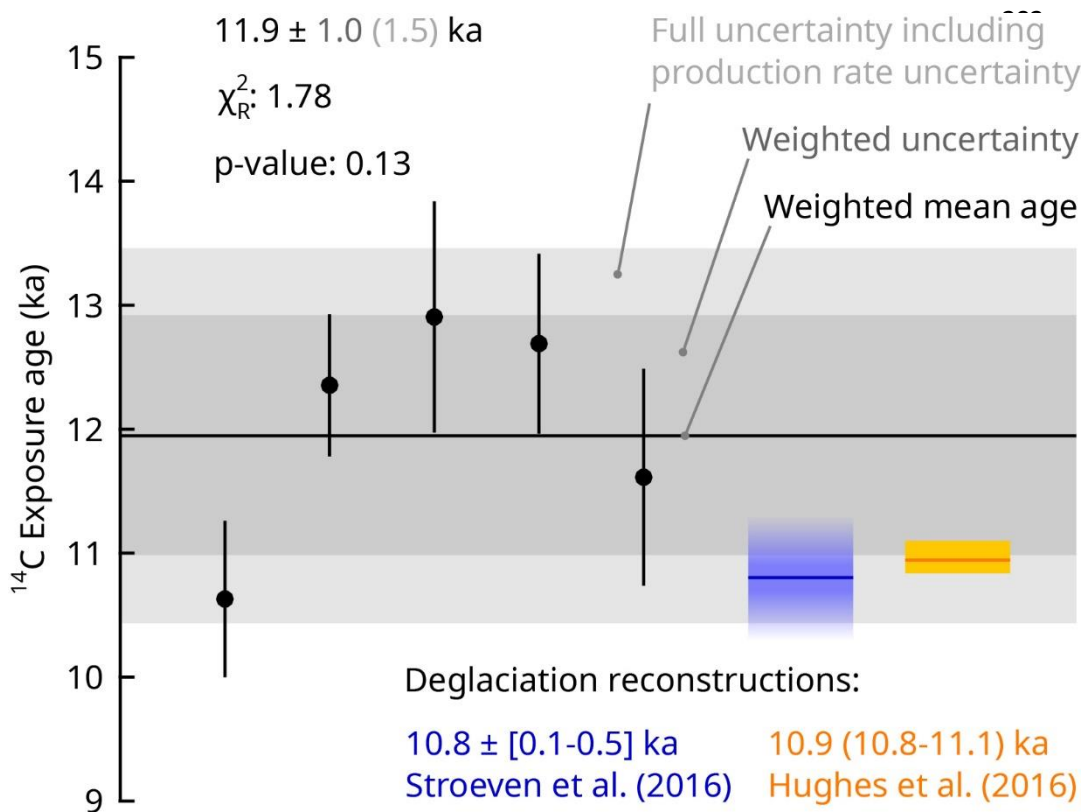
275 the Holocene RSL curve for Forsmark and the expected *in situ* ^{14}C exposure age curve considering
 276 subaqueous cosmogenic nuclide production (Figure 3; Table 2). Exposure age uncertainties are large
 277 with internal uncertainties (measurement uncertainties; Balco et al., 2008) of 5-9% and external
 278 uncertainties of 13-25% (also including production rate uncertainties, which are high relative to ^{10}Be
 279 (Borchers et al., 2016; Phillips et al., 2016). Apparent exposure ages increase consistently with elevation
 280 and match expected ages within uncertainty. The two highest samples have near-identical apparent
 281 exposure ages and elevations. However, these samples provide independent ages because they are
 282 horizontally separated by 624 m (Figure 1b). There is good agreement between ages inferred from these
 283 *in situ* ^{14}C data and the RSL curve constructed from organic radiocarbon dating of isolation events
 284 (Hedenström and Risberg, 2003; SKB, 2020).



285
 286 **Figure 3.** Apparent ^{14}C exposure ages for five Forsmark samples from below the highest shoreline (Fig.
 287 1b; Table 2) with 1σ external uncertainties. The expected exposure ages are calculated assuming the RSL
 288 curve is correct, the ^{14}C spallation production rate is correct, partial exposure as the sample approaches
 289 the water surface, and full post-glacial exposure for the duration above sea level. Hence, the expected
 290 exposure age curve is a few hundred years older than the RSL curve. The RSL curve is from SKB (2020)
 291 and uncertainties for the 1–6 ka interval are calculated from the original radiocarbon data in Hedenström
 292 and Risberg (2003). The RSL uncertainty envelope is also transposed onto the expected exposure age
 293 curve.

294 Apparent exposure ages for the five *in situ* ^{14}C samples located above the highest shoreline in Dalarna
 295 and Gävleborg (Fig. 1a) are shown in Figure 4 and Table 2. The weighted mean age from all five samples
 296 is 11.9 ± 1.5 ka. These data display a χ_R^2 of 1.78 and a p-value of 0.13 based on 1σ internal uncertainties,
 297 which does not support a rejection of the hypothesis that the apparent exposure ages represent the
 298 same population. In addition to the samples being from the same population, the exposure ages are
 299 consistent, within uncertainty, with the expected deglaciation age of 10.8 ± 0.3 ka (Stroeven et al. 2016).
 300 Replicate measurements on sample BG21-002 closely agree and an age based on a weighted mean ^{14}C
 301 concentration is shown in Figure 4.

302



315 **Figure 4.** Exposure ages from samples above the highest shoreline (Fig. 1a; Table 2). The individual
 316 samples (filled black circles) display 1σ internal uncertainty (measurement uncertainty; black lines). For
 317 the repeat sample BG21-002, the exposure age is calculated with a weighted mean ^{14}C concentration
 318 using a 2% uncertainty. The cosmogenic nuclide ages yield a reduced chi- square (χ_R^2) of 1.78 and a p-
 319 value of 0.13 based on internal uncertainties, which indicates that they are from the same population.
 320 The color gradient for the Stroeven et al. (2016) deglaciation chronology indicates the 0.1–0.5 ka
 321 uncertainty range, whereas the uncertainty for the Hughes et al. (2016) chronology reflects the
 322 maximum and minimum estimates for deglaciation of the study area, which are unequally distributed
 323 around the most credible estimate (orange line).

Table 1. *In situ* ¹⁴C sample measurement details

Sample	PCEGS ¹ #	PLID ²	Mass Quartz (g)	C yield (μg)	Diluted Mass C (μg)	AMS Split Mass C ³ (μg)	δ ¹³ C (‰ VPDB ⁴)	¹⁴ C/ ¹³ C ⁵ (10 ¹²)	¹⁴ C/C _{total} ⁶ (10 ¹⁴)	¹⁴ C ⁷ (10 ⁵ at)	[¹⁴ C] (10 ⁵ at g ⁻¹)	
BG21-001	PCEGS-146	202101960	5.02378	5.0 ± 0.1	393.8 ± 4.8	382.3 ± 4.6	-45.9 ± 0.2	3.3992 ± 0.0745	3.4118 ± 0.0785	6.1771 ± 0.1793	1.2296 ± 0.0357	
BG21-002	PCEGS-147	202101961	5.02383	7.8 ± 0.1	303.3 ± 3.7	294.4 ± 3.6	-44.8 ± 0.2	4.5548 ± 0.0964	4.6226 ± 0.1016	6.4703 ± 0.1806	1.2879 ± 0.0360	
BG21-002R	PCEGS-150	202201473	5.04116	7.7 ± 0.1	305.3 ± 3.7	296.4 ± 3.6	-45.2 ± 0.2	4.5575 ± 0.1350	4.6239 ± 0.1422	6.5186 ± 0.2368	1.2931 ± 0.0470	
BG21-003	PCEGS-148	202101962	5.01070	17.6 ± 0.3	303.4 ± 3.7	294.5 ± 3.6	-43.9 ± 0.2	4.6325 ± 0.1075	4.7091 ± 0.1134	6.6042 ± 0.1969	1.3180 ± 0.0393	
BG21-004	PCEGS-152	202101963	5.05927	11.9 ± 0.2	305.7 ± 3.7	296.8 ± 3.6	-44.6 ± 0.2	4.6181 ± 0.0789	4.6905 ± 0.0832	6.6300 ± 0.1588	1.3105 ± 0.0314	
BG21-005	PCEGS-153	202101964	5.07578	4.6 ± 0.1	304.5 ± 3.7	295.6 ± 3.6	-45.4 ± 0.2	4.5997 ± 0.1272	4.6668 ± 0.1339	6.5656 ± 0.2251	1.2935 ± 0.0444	
BG21-006	PCEGS-155	202101965	5.06572	5.5 ± 0.1	306.8 ± 3.7	297.8 ± 3.6	-45.2 ± 0.2	1.2766 ± 0.0562	1.1715 ± 0.0594	1.2426 ± 0.1010	0.2453 ± 0.0199	
BG21-007	PCEGS-157	202101966	5.03589	6.9 ± 0.1	309.2 ± 3.8	300.1 ± 3.7	-45.0 ± 0.2	1.6838 ± 0.0507	1.6007 ± 0.0536	1.9221 ± 0.0960	0.3817 ± 0.0191	
BG21-008	PCEGS-158	202101967	5.07653	4.0 ± 0.1	308.9 ± 3.8	299.9 ± 3.6	-45.4 ± 0.2	2.3565 ± 0.0634	2.3076 ± 0.0669	3.0145 ± 0.1185	0.5938 ± 0.0234	
BG21-009	PCEGS-160	202101968	5.01906	55.3 ± 0.7	305.6 ± 3.7	296.6 ± 3.6	-38.0 ± 0.2	3.3393 ± 0.0946	3.3681 ± 0.1005	4.6013 ± 0.1703	0.9168 ± 0.0339	
BG21-010	PCEGS-161	202101969	4.99961	42.2 ± 0.6	306.0 ± 3.7	297.0 ± 3.6	-40.1 ± 0.2	3.3197 ± 0.0680	3.3399 ± 0.0721	4.5648 ± 0.1321	0.9130 ± 0.0264	
Procedural Blanks												
PB2-03222022	PCEGS-135	202201450	--	1.4 ± 0.1	305.2 ± 3.7	296.2 ± 3.6	-40.2 ± 0.2	0.4863 ± 0.0298	0.3413 ± 0.0320	0.5222 ± 0.0493	--	
PB2-04212022	PCEGS-145	202201452	--	1.8 ± 0.1	307.0 ± 3.7	298.0 ± 3.6	-46.0 ± 0.2	0.5182 ± 0.0273	0.3731 ± 0.0292	0.5742 ± 0.0455	--	
PB2-05212022	PCEGS-163	202201454	--	2.3 ± 0.1	307.4 ± 3.7	298.4 ± 3.6	-46.0 ± 0.2	0.5364 ± 0.0315	0.3922 ± 0.0335	0.6045 ± 0.0521	--	
PB2-06022022	PCEGS-169	202201459	--	2.3 ± 0.1	307.3 ± 3.7	298.3 ± 3.6	-40.3 ± 0.2	0.4920 ± 0.0291	0.3486 ± 0.0312	0.5371 ± 0.0486	--	
								<i>Mean ± 1σ (All blanks)</i>	<i>0.5595 ± 0.0371</i>			
								<i>Mean ± 1σ (145, 163 only)</i>	<i>0.5894 ± 0.0214</i>			

Notes

- 1 Purdue Carbon Extraction and Graphitization System.
- 2 Prime Lab ID.
- 3 Mass graphitized for AMS analysis after small aliquot (ca. 9 μg C) taken for stable C isotopic analysis offline.
- 4 VPDB is Vienna Pee Dee Belemnite.
- 5 Measured relative to OX-2 standard.
- 6 Corrected for mass-dependent graphitization blank (based on AMS Split Mass C) and stable C composition.
- 7 Sample values calculated using Diluted Mass C and corrected for mean procedural blank (All blanks).

Table 2. Apparent *in situ* ^{14}C ages from quartz, Dalarna-Gävleborg and Forsmark-Uppland.

Sample ¹	Lat (°)	Long (°)	Elevation (m a.s.l.)	^{14}C age ² (ka)
BG21-001	60.47432	16.33134	236.5	10.6 ± 2.2 (± 0.6)
BG21-002	60.40615	16.22197	212.6	12.3 ± 2.9 (± 0.8)
BG21-002R	60.40615	16.22197	212.6	12.4 ± 3.0 (± 1.1)
BG21-003	60.38459	16.17649	216.3	12.9 ± 3.2 (± 0.9)
BG21-004	60.38451	16.17440	217.8	12.7 ± 3.0 (± 0.7)
BG21-005	60.36888	16.30526	248.1	11.6 ± 2.6 (± 0.9)
BG21-006	60.38490	18.22308	9.4	1.5 ± 0.2 (± 0.1)
BG21-007	60.37892	18.19129	12.2	2.6 ± 0.3 (± 0.2)
BG21-008	60.30504	18.04993	30.3	4.5 ± 0.6 (± 0.2)
BG21-009	60.22988	17.94989	56.0	8.2 ± 1.5 (± 0.5)
BG21-010	60.22431	17.95051	55.9	8.2 ± 1.4 (± 0.4)

Notes

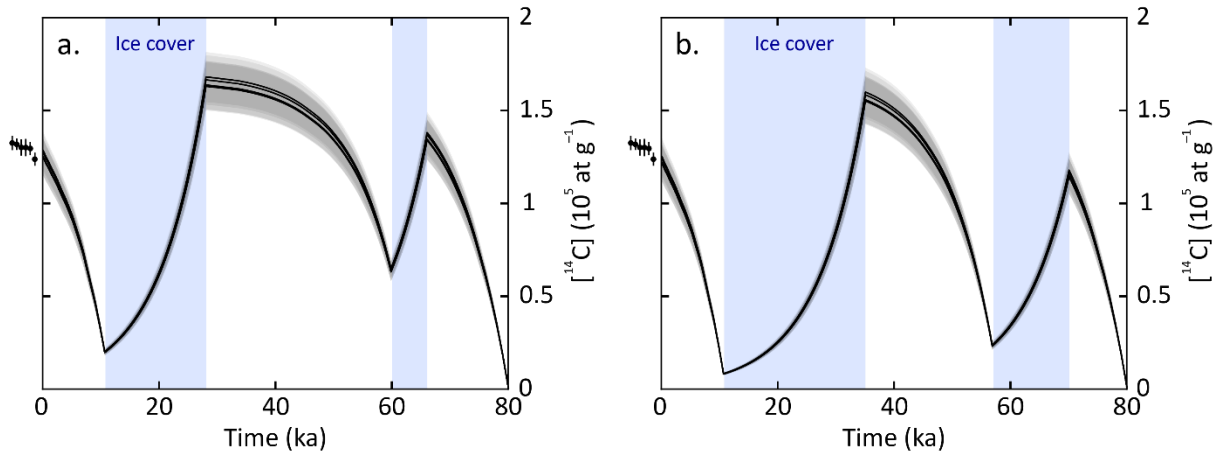
- 1 All samples have a thickness of 3 cm, a density of 2.7 g cm⁻³, and a shielding factor of 1. Zero erosion is assumed.
- 2 ^{14}C age and 1 σ external uncertainty (1 σ internal uncertainty).

328 5. Discussion

329 The *in situ* ^{14}C bedrock exposure ages from the Forsmark-Uppland transect (i.e., below the highest
330 postglacial shoreline) consistently increase with elevation and overlap the expected exposure age
331 curve, within uncertainty (Fig. 3). This study adds to precious few applications of cosmogenic nuclides
332 to defining postglacial landscape emergence above sea level (Briner et al., 2006; Bierman et al., 2018).
333 Briner et al. (2006) present good (visual) congruence with a record of shoreline emergence built from
334 radiocarbon-dated driftwood and fauna by Dyke et al. (1992) using ^{10}Be measurements on boulders in
335 beaches derived from wave-washed till. Their study also mentions that building a relative sea level
336 curve from pebbles, cobbles and plucked bedrock suffered from inheritance problems, an experience
337 shared by Matmon et al. (2003) while attempting the dating of chert on beach ridges in southern Israel
338 and heeded by Bierman et al. (2018). Bierman et al. (2018) successfully dated landscape emergence on
339 Greenland using ^{10}Be across a range of settings, including bedrock below the highest shoreline, cobbles
340 from beach ridges at the highest shoreline, and boulders and bedrock above the highest shoreline.
341 They note that success hinges on the requirement of warm-based ice and deep glacial erosion in
342 exposing bedrock devoid of an inherited cosmogenic nuclide inventory. In many regions, however,
343 including east-central Sweden and more widely in Fennoscandia, these requirements are not met
344 either because of cold-based conditions (Patton et al., 2016; Stroeven et al., 2016) or weakly erosive
345 warm-based ice such as at Forsmark (Hall et al., 2019; SKB, 2020), during all or much of glacial time.
346 Cosmogenic nuclide inheritance is therefore a part of the landscape fabric. Bierman et al. (2018)
347 advocate the use of *in situ* ^{14}C as a methodology to circumvent inheritance problems. Our study is the
348 first to follow-up on that suggestion, and shows, convincingly, that using *in situ* ^{14}C can extend the study
349 of landscape rebound to regions where ice sheet erosion was insufficiently deep to allow for the
350 application of long-lived nuclides.

351 Five bedrock samples from above the highest postglacial shoreline are well-clustered and the weighted
352 mean age (and full uncertainty) of 11.9 ± 1.5 ka overlaps with the predicted deglaciation age of $10.8 \pm$
353 0.3 ka (Fig. 4; Hughes et al., 2016; Stroeven et al., 2016). Because derived exposure ages overlap with
354 the predicted deglaciation age, we further infer that the *in situ* ^{14}C samples, including those located
355 below the highest postglacial shoreline, within uncertainty, lack significant inheritance from previous
356 exposure. Model scenarios of *in situ* ^{14}C concentration evolution over varying durations of MIS2 and
357 MIS4 ice cover are consistent with minor inheritance, even with short periods of ice coverage and no
358 glacial or interglacial erosion (Figure 5). Even if the last ice sheet had advanced over the region as late

359 as 28 ka BP, there would only be a negligible inventory of inherited ^{14}C atoms produced prior to the
360 MIS2 ice advance.



361 **Figure 5.** Modelled *in situ* ^{14}C concentration evolution over the last 80 kyr in the five samples (BG21-
362 001– BG21-005) from above the highest shoreline. The ^{14}C development is modelled assuming no
363 glacial or interglacial erosion, continuous exposure to cosmic rays during ice-free periods, and full
364 shielding from cosmic rays (no ^{14}C production) during periods with ice cover. The points just left of the
365 plots display the measured ^{14}C concentrations for the six sample measurements (Table 1). (a) Scenario
366 with short periods of MIS4 and MIS2 ice cover from 66 to 60 ka BP and from 28 ka BP to deglaciation
367 around 10.7 ka BP. (b) Scenario with longer periods of MIS4 and MIS2 ice cover from 70 to 57 ka BP and
368 from 35 ka BP to the deglaciation around 10.7 ka BP. Due to the rapid decay of ^{14}C (half-life of $5700 \pm$
369 30 years), both scenarios yield similar end-point concentrations of ^{14}C that overlap, within
370 uncertainties, the measured sample concentrations.

371 Our *in situ* ^{14}C data from above the highest (postglacial) shoreline demonstrate their potential for
372 constraining the deglaciation chronology of former ice sheets. This is especially true for regions with
373 thin till drapes, abundant bedrock exposures, and sparse moraines outlining successive retreat stages.
374 In Fennoscandia, thin tills occur commonly (cf. Kleman et al., 2008) and ice sheet retreat appears to
375 have proceeded uninterrupted inside the Younger Dryas moraine belt (apart from the Central Finland
376 Ice-Marginal Formation; e.g., Rainio et al., 1986; Stroeven et al., 2016). Whereas the post-Younger
377 Dryas deglaciation of east-central Sweden is well constrained by clay-varve chronology below the
378 highest postglacial shoreline (Strömberg, 1989), there are vast areas above the highest shoreline that
379 remain poorly constrained by data (Stroeven et al. 2016). In addition to a lack of datable deglacial
380 landforms, this is attributable to glacial erosion of bedrock having frequently been insufficient to
381 remove inventories of long half-life ^{10}Be and ^{26}Al (Patton et al., 2022), thereby leaving nuclides inherited
382 from exposure prior to the last glaciation (Heyman et al., 2011; Stroeven et al., 2016). Because of the
383 short ^{14}C half-life and an improved sampling methodology, *in situ* ^{14}C may now be a prime candidate
384 nuclide to be included in last deglaciation studies on glaciated cratons, such as the dating of boulders

385 deposited along glacial flowlines; a technique practiced successfully using ^{10}Be (Margold et al., 2019;
386 Norris et al., 2022).

387

388 6. Conclusion

389 Ten *in situ* ^{14}C measurements on bedrock are consistent with a RSL curve for Forsmark derived from
390 organic radiocarbon dating of basal sediments in isolation basins and the Fennoscandian Ice Sheet
391 deglaciation chronologies from Stroeven et al. (2016) and Hughes et al. (2016). This study introduces
392 the use of *in situ* ^{14}C in Fennoscandian Ice Sheet paleoglaciology and outlines a promise of its use as a
393 basis for supporting future shoreline displacement studies and for tracking the deglaciation in areas
394 that lack datable organic material and where ^{10}Be and ^{26}Al routinely return complex exposure results.

395

396 **Data availability.** Data are available in Supplements 1-3. LiDAR data used in the study are available
397 from <https://www.lantmateriet.se>

398 **Author contributions.** BWG and APS initiated the study, with support from KH and JON, and drafted
399 the manuscript. BWG, APS, and AL did the sampling. AL did petrological analyses of the sampled
400 bedrock. NAL completed sample preparation for AMS and provided the results. JH carried out
401 cosmogenic nuclide production rate and exposure age calculations. MWC oversaw the AMS. All
402 authors revised the manuscript.

403 **Competing interests.** The contact author has declared that none of the authors has any competing
404 interests.

405 **Disclaimer.** Publisher's note: Copernicus Publications remains neutral with regard to jurisdictional
406 claims in published maps and institutional affiliations.

407 **Acknowledgements.** We thank Johan Liakka (SKB) for his support in completing this study and
408 Nicolás Young and an anonymous reviewer for comments that improved this manuscript.

409 **Financial support.** This research was supported by the Swedish Nuclear Fuel and Waste Management
410 Company.

411 **Review statement.** This paper was edited by Pieter Vermeesch and reviewed by Nicolás Young and
412 an anonymous reviewer.

413 References

414 Alexanderson, H., Hättestrand, M., Lindqvist, M. A., Sigfusdottir, T.: MIS 3 age of the Veiki moraine in
415 N Sweden - Dating the landform record of an intermediate-sized ice sheet in Scandinavia, Arctic,
416 Antarctic, and Alpine Research, 54, 239-261, 2022.

417 Balco, G., Stone, J. O., Lifton, N. A., Dunai, T. J.: A complete and easily accessible means of calculating
418 surface exposure ages or erosion rates from ^{10}Be and ^{26}Al measurements, Quaternary
419 Geochronology, 3, 174-195, 2008.

420 Berglund, M.: The Holocene shore displacement of Gästrikland, eastern Sweden: a contribution to
421 the knowledge of Scandinavian glacio-isostatic uplift, *Journal of Quaternary Science*, 20, 519–531,
422 2005.

423 Bergström, E.: Late Holocene distribution of lake sediment and peat in NE Uppland, Sweden, SKB R-
424 01-12, Svensk Kärnbränslehantering AB, 2001.

425 Bierman, P. R., Rood, D. H., Shakun, J. D., Portenga, E. W., Corbett, L. B.: Directly dating postglacial
426 Greenlandic land-surface emergence at high resolution using *in situ* ^{10}Be , *Quaternary Research*, 90,
427 110-126, 2018.

428 Blake, Jr., W.: Holocene emergence along the Ellesmere Island coast of northernmost Baffin Bay,
429 *Norsk Geologisk Tidsskrift*, 73, 147–160, 1993.

430 Borchers, B., Marrero, S., Balco, G., Caffee, M., Goehring, B., Lifton, N., Nishiizumi, K., Phillips, F.,
431 Schaefer, J., Stone, J.: Geological calibration of spallation production rates in the CRONUS Earth
432 project, *Quaternary Geochronology*, 31, 188–198, 2016.

433 Bradwell, T., Fabel, D., Clark, C. D., Chiverrell, R. C., Small, D., Smedley, R. K., Saher, M. H., Moreton,
434 S. G., Dove, D., Callard, S. L., Duller, G. A. T., Medialdea, A., Bateman, M. D., Burke, M. J., McDonald,
435 N., Gilgannon, S., Morgan, S., Roberts, D. H., Ó Cofaigh, C.: Pattern, style and timing of British-Irish Ice
436 Sheet advance and retreat over the last 45 000 years: evidence from NW Scotland and the adjacent
437 continental shelf, *Journal of Quaternary Science*, 36, 871–933, 2021.

438 Briner, J. P., Gosse, J. C., Bierman, P. R.: Applications of cosmogenic nuclides to Laurentide Ice Sheet
439 history and dynamics, *Geological Society of America, Special Paper*, 415, 29-41, 2006.

440
441 Briner, J. P., Lifton, N. A., Miller, G. H., Refsnider, K., Anderson, R. K., Finkel, R.: Using *in situ*
442 cosmogenic ^{10}Be , ^{14}C , and ^{26}Al to decipher the history of polythermal ice sheets, *Quaternary*
443 *Geochronology*, 19, 4–13, 2014.

444 Brunnberg, L.: Clay-varve Chronology and Deglaciation during the Younger Dryas and Preboreal in the
445 Easternmost Part of the Middle Swedish Ice Marginal Zone, Department of Quaternary Research,
446 Quaternaria A2, Stockholm University, Stockholm, 1-94, 1995.

447 Dalton, A.S., Dulfer, H.E., Margold, M., Heyman, J., Clague, J.J., Froese, D.G., Gauthier, M.S., Hughes,
448 A.L.C., Jennings, C.E., Norris, S.L., Stoker, B.J.: Deglaciation of the north American ice sheet complex
449 in calendar years based on a comprehensive database of chronological data: NADI-1, *Quaternary*
450 *Science Reviews*, 321, 108345, 2023.

451 Dalton, A. S., Margold, M., Stokes, C. R., Tarasov, L., Dyke, A. S., Adams, R. S., Allard, S., Arends, H. E.,
452 Atkinson, N., Attig, J. W., Barnett, P. J., Barnett, R. L., Batterson, M., Bernatchez, P., Borns Jr., H. W.,
453 Breckenridge, A., Briner, J. P., Brouard, E., Campbell, J. E., Carlson, A. E., Clague, J. J., Curry, B. B.,
454 Daigneault, R. A., Dubé-Loubert, H., Easterbrook, D. J., Franzi, D. A., Friedrich, H. G., Funder, S.,
455 Gauthier, M. S., Gowan, A. S., Harris, K. L., Hétu, B., Hooyer, T. S., Jennings, C. E., Johnson, M. D.,
456 Kehew, A. E., Kelley, S. E., Kerr, D., King, E. L., Kjeldsen, K. K., Knaeble, A. R., Lajeunesse, P., Lakeman,
457 T. R., Lamothe, M., Larson, P., Lavoie, M., Loope, H. M., Lowell, T. V., Lusardi, B. A., Manz, L.,
458 McMartin, I., Nixon, F. C., Occhietti, S., Parkhill, M. A., Piper, D. J. W., Pronk, A. G., Richard, P. J. H.,
459 Ridge, J. C., Ross, M., Roy, M., Seaman, A., Shaw, J., Stea, R. R., Teller, J. T., Thompson, W. B.,
460 Thorleifson, L. H., Utting, D. J., Veillette, J. J., Ward, B. C., Weddle, T. K., Wright, H. E.: An updated
461 radiocarbon-based ice margin chronology for the last deglaciation of the North American Ice Sheet
462 Complex, *Quaternary Science Reviews*, 234, 106223, 2020.

- 463 De Geer, G.: The transbaltic extension of the Swedish Time Scale, *Geografiska Annaler*, 17, 533-549,
464 1935.
- 465 De Geer, G.: *Geochronologia Suecica* principles, *Kungliga svenska vetenskapsakademien Handlingar*,
466 III, Bd 18, 6, 1–367, 1940.
- 467 Dyke, A. S., Morris, T. F., Green, D. E. C., England, J.: Quaternary geology of Prince of Wales Island,
468 Arctic Canada, *Geological Survey of Canada, Memoir*, 433, 1–142, 1992.
- 469 Dyke, A. S., Andrews, J. T., Clark, P. U., England, J. H., Miller, G. H., Shaw, J., Veillette, J. J.: The
470 Laurentide and Innuitian ice sheets during the Last Glacial Maximum, *Quaternary Science Reviews*,
471 21, 9–31, 2002.
- 472 Fogwill, C., Turney, C., Golledge, N., Rood, D., Hippe, K., Wacker, L., Jones, R.: Drivers of abrupt
473 Holocene shifts in West Antarctic ice stream direction determined from combined ice sheet
474 modelling and geologic signatures. *Antarctic Science*, 26, 674–686, 2014.
- 475 Goehring, B. M., Schaefer, J. M., Schluechter, C., Lifton, N. A., Finkel, R. C., Jull, A. J. T., Akçar, N.,
476 Alley, R. B.: The Rhone Glacier was smaller than today for most of the Holocene, *Geology*, 39, 679–
477 682, 2011.
- 478 Gosse, J. C., Phillips, F. M.: Terrestrial *in situ* cosmogenic nuclides: theory and application, *Quaternary
479 Science Reviews*, 20, 1475–1560, 2001.
- 480 Greenwood, S. L., Simkins, L. M., Winsborrow, M. C. M., Bjarnadottir, L. R.: Exceptions to bed-
481 controlled ice sheet flow and retreat from glaciated continental margins worldwide, *Science
482 Advances*, 7, eabb6291, 2021.
- 483 Greenwood, S. L., Clason, C. C., Nyberg, J., Jakobsson, M., Holmlund, P.: The Bothnian Sea ice stream:
484 early Holocene retreat dynamics of the south-central Fennoscandian Ice Sheet, *Boreas*, 46, 346-362,
485 2017.
- 486 Hall A. M., Ebert K., Goodfellow B. W., Hättestrand C., Heyman J., Krabbendam M., Moon S., Stroeven
487 A. P.: Past and future impact of glacial erosion in Forsmark and Uppland. TR-19-07 Svensk
488 Kärnbränslehantering AB, 2019.
- 489 Hall, A. M., Krabbendam, M., van Boeckel, M., Goodfellow, B. W., Hättestrand, C., Heyman, J.,
490 Palamakumbura, R. N., Stroeven A. P., Näslund, J.-O.: Glacial ripping: geomorphological evidence
491 from Sweden for a new process of glacial erosion, *Geografiska Annaler*, 102, 333-353, 2020.
- 492 Hedenström, A., Risberg, J.: Shore displacement in northern Uppland during the last 6500 calendar
493 years, TR-03-17 Svensk Kärnbränslehantering AB, 2003.
- 494 Heyman, J., Stroeven, A. P., Harbor, J. M., Caffee, M. W.: Too young or too old: Evaluating
495 cosmogenic exposure dating based on an analysis of compiled boulder exposure ages, *Earth and
496 Planetary Science Letters*, 302, 71–80, 2011.
- 497 Hippe, K., Lifton, N. A.: Calculating isotope ratios and nuclide concentrations for *in situ* cosmogenic
498 ^{14}C Analyses, *Radiocarbon*, 56, 1167–1174, 2014.
- 499 Hippe, K., Ivy-Ochs, S., Kober, F., Zasadni, J., Wieler, R., Wacker, L., Kubik, P.W., Schlüchter, C.:
500 Chronology of Lateglacial ice flow reorganization and deglaciation in the Gotthard Pass area, Central
501 Swiss Alps, based on cosmogenic ^{10}Be and *in situ* ^{14}C , *Quaternary Geochronology*, 19, 14–26, 2014.

502 Hughes, A. L. C., Gyllencreutz, R., Lohne, Ø. S., Mangerud, J., Svendsen, J. I.: The last Eurasian ice
503 sheets – a chronological database and time-slice reconstruction, *DATED-1, Boreas*, 45, 1–45, 2016.

504 Ivy-Ochs, S., Kober, F.: Surface exposure dating with cosmogenic nuclides, *Quaternary Science*
505 *Journal*, 57, 157–189, 2008.

506 Kleman, J., Hättestrand, M., Borgström, I., Preusser, F., Fabel, D.: The Idre marginal moraine—an
507 anchorpoint for Middle and Late Weichselian ice sheet chronology, *Quaternary Science Advances*, 2,
508 100010, 2020.

509 Kleman, J., Stroeven, A. P., Lundqvist, J.: Patterns of Quaternary ice sheet erosion and deposition in
510 Fennoscandia and a theoretical framework for explanation, *Geomorphology*, 97, 73–90, 2008.

511 Koester, A., Lifton, N. A.: Technical note: A software framework for calculating compositionally
512 dependent *in situ* ¹⁴C production rates, *Geochronology*, 5, 21–33, 2023.

513 Lal, D.: Cosmic ray labeling of erosion surfaces: *in situ* nuclide production rates and erosion rates,
514 *Earth and Planetary Science Letters*, 104, 424–439, 1991.

515 Lambeck, K., Purcell, A., Zhao, J., Svensson, N.-O.: The Scandinavian Ice Sheet: from MIS 4 to the end
516 of the Last Glacial Maximum, *Boreas*, 39, 410–435, 2010.

517 Lambeck, K., Smither, C., Johnston, P.: Sea-level change, glacial rebound and mantle viscosity for
518 northern Europe, *Geophysical Journal International*, 134, 102–134, 1998.

519 Lidberg, M., Johansson, J. M., Scherneck, H.-G., Milne, G. A.: Recent results based on continuous GPS
520 observations of the GIA process in Fennoscandia from BIFROST, *Journal of Geodynamics*, 50, 8–18,
521 2010.

522 Lifton, N.: Implications of two Holocene time-dependent geomagnetic models for cosmogenic nuclide
523 production rate scaling, *Earth and Planetary Science Letters*, 433, 257–268, 2016.

524 Lifton, N., Caffee, M., Finkel, R., Marrero, S., Nishiizumi, K., Phillips, F. M., Goehring, B., Gosse, J.,
525 Stone, J., Schaefer, J., Theriault, B.: *In situ* cosmogenic nuclide production rate calibration for the
526 CRONUS-Earth project from Lake Bonneville, Utah, shoreline features, *Quaternary Geochronology*,
527 26, 56–69, 2015.

528 Lifton, N., Sato, T., and Dunai, T. J.: Scaling *in situ* cosmogenic nuclide production rates using
529 analytical approximations to atmospheric cosmic-ray fluxes, *Earth and Planetary Science Letters*, 386,
530 149–160, 2014.

531 Lifton, N., Wilson, J., Koester, A.: Technical note: Studying Li-metaborate fluxes and extraction
532 protocols with a new, fully automated *in situ* cosmogenic ¹⁴C processing system at PRIME Lab,
533 *Geochronology*, 5, 361–375, 2023.

534 Long, A. J., Woodroffe, S. A., Roberts, D. H., Dawson, S.: Isolation basins, sea-level changes and the
535 Holocene history of the Greenland Ice Sheet, *Quaternary Science Reviews*, 30, 3748–3768, 2011.

536 Lönnqvist, M., Hökmark, H.: Approach to estimating the maximum depth for glacially induced
537 hydraulic jacking in fractured crystalline rock at Forsmark, Sweden, *Journal of Geophysical Research:*
538 *Earth Surface*, 118, 1777–1791, 2013.

539 Lupker, M., Hippe, K., Wacker, L., Kober, F., Maden, C., Braucher, R., Bourlès, D., Romani, J. R. V.,
540 Wieler, R.: Depth-dependence of the production rate of *in situ* ¹⁴C in quartz from the Leymon High
541 core, Spain, *Quaternary Geochronology*, 28, 80–87, 2015.

- 542 Margold, M., Gosse, J. C., Hidy, A. J., Woywitka, R. J., Young, J. M., Froese, D.: Beryllium-10 dating of
543 the Foothills Erratics Train in Alberta, Canada, indicates detachment of the Laurentide Ice Sheet from
544 the Rocky Mountains at ~15 ka, *Quaternary Research*, 92, 469–482, 2019.
- 545 Marrero, S. M., Phillips, F. M., Caffee, M. W., Gosse, J. C.: CRONUS-Earth cosmogenic ^{36}Cl calibration,
546 *Quaternary Geochronology*, 31, 199–219, 2016.
- 547 Matmon, A., Crouvi, O., Enzel, Y., Bierman, P., Larsen, J., Porat, N., Amit, R., Caffee, M.: Complex
548 exposure histories of chert clasts in the late Pleistocene shorelines of Lake Lisan, southern Israel.
549 *Earth Surface Processes and Landforms* 28, 493–506, 2003.
- 550 Miller, G. H., Briner, J. P., Lifton, N. A., Finkel, R. C.: Limited ice-sheet erosion and complex exposure
551 histories derived from *in situ* cosmogenic ^{10}Be , ^{26}Al , ^{14}C on Baffin Island, Arctic Canada, *Quaternary*
552 *Geochronology*, 1, 74–85, 2006.
- 553 Moon, S., Perron, J. T., Martel, S.J., Goodfellow, B.W., Mas Ivars, D., Hall, A., Heyman, J., Munier, R.,
554 Näslund, J.-O., Simeonov, A., Stroeven, A.P.: Present-day stress field influences bedrock fracture
555 openness deep into the subsurface. *Geophysical Research Letters* 47, e2020GL090581, 2020.
- 556 Norris, S. L., Tarasov, L., Monteath, A. J., Gosse, J. C., Hidy, A. J., Margold, M., Froese, D. G.: Rapid
557 retreat of the southwestern Laurentide Ice Sheet during the Bølling-Allerød interval, *Geology*, 50,
558 417–421, 2022.
- 559 Påsse, T., Andersson, L: Shore-level displacement in Fennoscandia calculated from empirical data,
560 *GFF*, 127, 253–268, 2005.
- 561 Patton, H., Hubbard, A., Andreassen, K., Auriac, A., Whitehouse, P. L., Stroeven, A. P., Shackleton, C.,
562 Winsborrow, M., Heyman, J., Hall, A. M.: Deglaciation of the Eurasian ice sheet complex, *Quaternary*
563 *Science Reviews*, 169, 148–172, 2017.
- 564 Patton, H., Hubbard, A., Andreassen, K., Winsborrow, M., Stroeven, A.P.: The build-up, configuration,
565 and dynamical sensitivity of the Eurasian ice-sheet complex to Late Weichselian climatic and oceanic
566 forcing, *Quaternary Science Reviews*, 153, 97–121, 2016.
- 567 Patton, H., Hubbard, A., Heyman, J., Alexandropoulou, N., Lasabuda, A. P. E., Stroeven, A.P., Hall,
568 A.M., Winsborrow, M., Sugden, D.E., Kleman, J., Andreassen, K.: The extreme yet transient nature of
569 glacial erosion, *Nature Communications* 13, 7377, 2022.
- 570 Pendleton, S., Miller, G., Lifton, N., Young, N.: Cryosphere response resolves conflicting evidence for
571 the timing of peak Holocene warmth on Baffin Island, Arctic Canada, *Quaternary Science*
572 *Reviews*, 216, 107–115, 2019.
- 573 Phillips, F. M., Argento, D. C., Balco, G., Caffee, M. W., Clem, J., Dunai, T. J., Finkel, R., Goehring, B.,
574 Gosse, J. C., Hudson, A. M., Jull, A. J. T., Kelly, M. A., Kurz, M., Lal, D., Lifton, N., Marrero, S. M.,
575 Nishiizumi, K., Reedy, R. C., Schaefer, J., Stone, J. O. H., Swanson, T., Zreda, M. G.: The CRONUS-Earth
576 Project: A synthesis, *Quaternary Geochronology*, 31, 119–154, 2016.
- 577 Rainio, H., Kejonen, A., Kielosto, S., Lahermo, P.: Avancerade inlandsisen på nytt också till
578 Mellanfinska randformationen? *Geologi*, 38, 95–109, 1986.
- 579 Regnéll, C., Becher, G. P., Öhrling, C., Greenwood, S. L., Gyllencreutz, R., Blomdin, R., Brendryen, J.,
580 Goodfellow, B. W., Mikko, H., Ransed, G., Smith, C.: Ice-dammed lakes and deglaciation history of the
581 Scandinavian Ice Sheet in central Jämtland, Sweden, *Quaternary Science Reviews*, 314, 108219, 2023.

- 582 Risberg, J.: Strandförskjutningen i nordvästra Uppland under subboreal tid. In Segerberg, A. Bälinge
583 mossar: kustbor i Uppland under yngre stenålder, PhD Thesis. Uppsala University, Appendix 4. (in
584 Swedish), 1999.
- 585 Robertsson, A.-M., Persson, C.: Biostratigraphical studies of three mires in northern Uppland,
586 Sweden, Sveriges geologiska undersökning, (Serie C 821.), 1989.
- 587 Romundset, A., Bondevik, S., Bennike, O.: Postglacial uplift and relative sea level changes in
588 Finnmark, northern Norway, Quaternary Science Reviews, 30, 2398–2421, 2011.
- 589 Schildgen, T. F., Phillips, W. M., Purves, R. S.: Simulation of snow shielding corrections for cosmogenic
590 nuclide surface exposure studies, Geomorphology, 64, 67–85, 2005.
- 591 Schimmelpfennig, I., Schaefer, J. M., Goehring, B. M., Lifton, N., Putnam, A. E., Barrell, D. J.:
592 Calibration of the *in situ* cosmogenic ¹⁴C production rate in New Zealand's Southern Alps, Journal of
593 Quaternary Science, 27, 671–674, 2012.
- 594 Schimmelpfennig, I., Schaefer, J. M., Lamp, J., Godard, V., Schwartz, R., Bard, E., Tuna, T., Akçar, N.,
595 Schlüchter, C., Zimmerman, S., and ASTER Team: Glacier response to Holocene warmth inferred from
596 *in situ* ¹⁰Be and ¹⁴C bedrock analyses in Steingletscher's forefield (central Swiss Alps), Climate of the
597 Past, 18, 23–44, 2022.
- 598 Schweinsberg, A. D., Briner, J. P., Miller, G. H., Lifton, N. A., Bennike, O., & Graham, B. L.: Holocene
599 mountain glacier history in the Sukkertoppen Iskappe area, southwest Greenland, Quaternary
600 Science Reviews, 197, 142–161, 2018.
- 601 SGU: Högsta Kustlinjen (in Swedish) [https://resource.sgu.se/dokument/produkter/hogsta-kustlinjen-](https://resource.sgu.se/dokument/produkter/hogsta-kustlinjen-beskrivning)
602 [beskrivning](https://resource.sgu.se/dokument/produkter/hogsta-kustlinjen-beskrivning) (Geological Survey of Sweden), 2015.
- 603 Simkins, L. M., Simms, A. R., DeWitt, R.: Relative sea-level history of Marguerite Bay, Antarctic
604 Peninsula derived from optically stimulated luminescence-dated beach cobbles, Quaternary Science
605 Reviews, 77, 141–155, 2013.
- 606 SKB: Post-closure safety for the final repository for spent nuclear fuel at Forsmark – Climate and
607 climate-related issues, PSAR version, TR-20-12, Svensk Kärnbränslehantering AB, 2020.
- 608 SKB: Post-closure safety for the final repository for spent nuclear fuel at Forsmark – Main report,
609 PSAR version. SKB TR-21-01, Svensk Kärnbränslehantering AB, 2022.
- 610 Steffen, H., Wu, P.: Glacial isostatic adjustment in Fennoscandia - A review of data and modeling,
611 Journal of Geodynamics, 52, 169–204, 2011.
- 612 Steinemann, O., Ivy-Ochs, S., Hippe, K., Christl, M., Haghpor, N., and Synal, H. A.: Glacial erosion by
613 the Trift glacier (Switzerland): Deciphering the development of riegels, rock basins and gorges,
614 Geomorphology, 375, 107533, 2021.
- 615 Stephens, M. B., Jansson, N. F.: Chapter 6, Paleoproterozoic (1.9–1.8 Ga) syn-orogenic magmatism,
616 sedimentation and mineralization in the Bergslagen lithotectonic unit, Svecokarelian orogen. In M B
617 Stephens & J Bergman Wehede (eds.): Sweden: Lithotectonic Framework, Tectonic Evolution and
618 Mineral Resources, Geological Society of London Memoirs, 50, 105–206, 2020.

- 619 Stroeven, A. P., Hättstrand, C., Kleman, J., Heyman, J., Fabel, D., Fredin, O., Goodfellow, B. W.,
620 Harbor, J. M., Jansen, J. D., Olsen, L., Caffee, M. W., Fink, D., Lundqvist, J., Rosqvist, G. C., Strömberg,
621 B., Jansson, K. N.: Deglaciation of Fennoscandia, *Quaternary Science Reviews*, 147, 91–112, 2016.
- 622 Stroeven, A.P., Heyman, J., Fabel, D., Björck, S., Caffee, M.W., Fredin, O., Harbor, J.M.: A new
623 Scandinavian reference ^{10}Be production rate, *Quaternary Geochronology*, 29, 104–115, 2015.
- 624 Strömberg, B.: Late Weichselian deglaciation and clay varve chronology in east-central Sweden,
625 *Sveriges geologiska undersökning (Ser. Ca 73)*, 1989.
- 626 Strömberg, B.: Younger Dryas deglaciation at Mt. Billingen, and clay varve dating of the Younger
627 Dryas/Preboreal transition, *Boreas*, 23, 177-193, 1994.
- 628 Wohlfarth, B., Björck, S., Possnert, G.: The Swedish Time Scale: a potential calibration tool for the
629 radiocarbon time scale during the late Weichselian, *Radiocarbon*, 37, 347-359, 1995.
- 630 Young, N. E., Lesnek, A. J., Cuzzone, J. K., Briner, J. P., Badgeley, J. A., Balter-Kennedy, A., Graham, B.
631 L., Cluett, A., Lamp, J. L., Schwartz, R., Tuna, T., Bard, E., Caffee, M. W., Zimmerman, S. R. H.,
632 Schaefer, J. M.: *In situ* cosmogenic ^{10}Be – ^{14}C – ^{26}Al measurements from recently deglaciated bedrock as
633 a new tool to decipher changes in Greenland Ice Sheet size, *Climate of the Past*, 17, 419–450, 2021.
- 634 Young, N. E., Schaefer, J. M., Goehring, B., Lifton, N., Schimmelpfennig, I., Briner, J. P.: West
635 Greenland and global *in situ* ^{14}C production-rate calibrations, *Journal of Quaternary Science*, 29, 401–
636 406, 2014.